Supplementary Information for:

Printable, Self-Healing and Recyclable PEDOT:PSS/Polyurethane Composites for Durable Bioelectronics

Jinsil Kim[1] and Fabio Cicoira[*]

[1]Department of Chemical Engineering, Polytechnique Montréal, Montréal, QC H3C 3A7, Canada

*Corresponding author. E-mail: fabio.cicoira@polymtl.ca

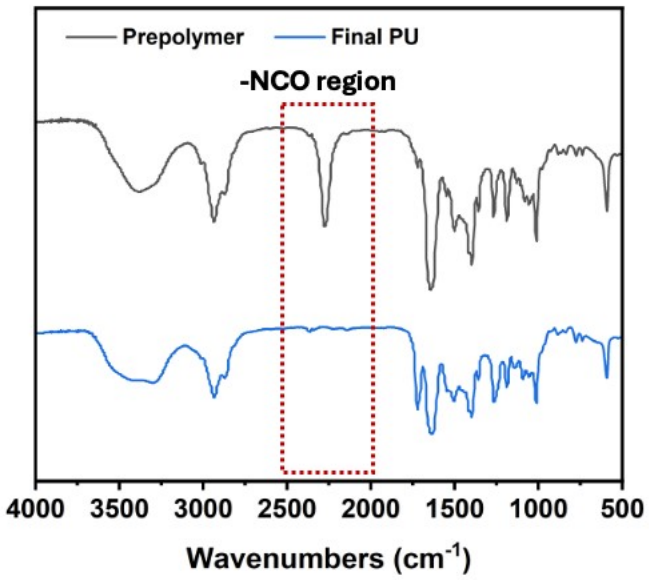

Figure S1. FTIR spectra of the prepolymer and the final polyurethane synthesized in this study.

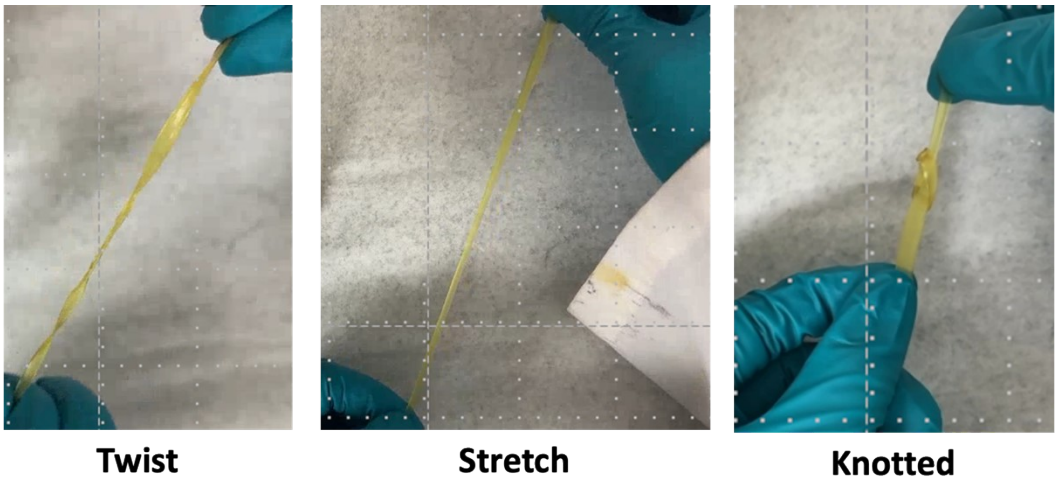

Figure S2. Photographs showing twisting, stretching, and knotting behavior of the synthesized PU.

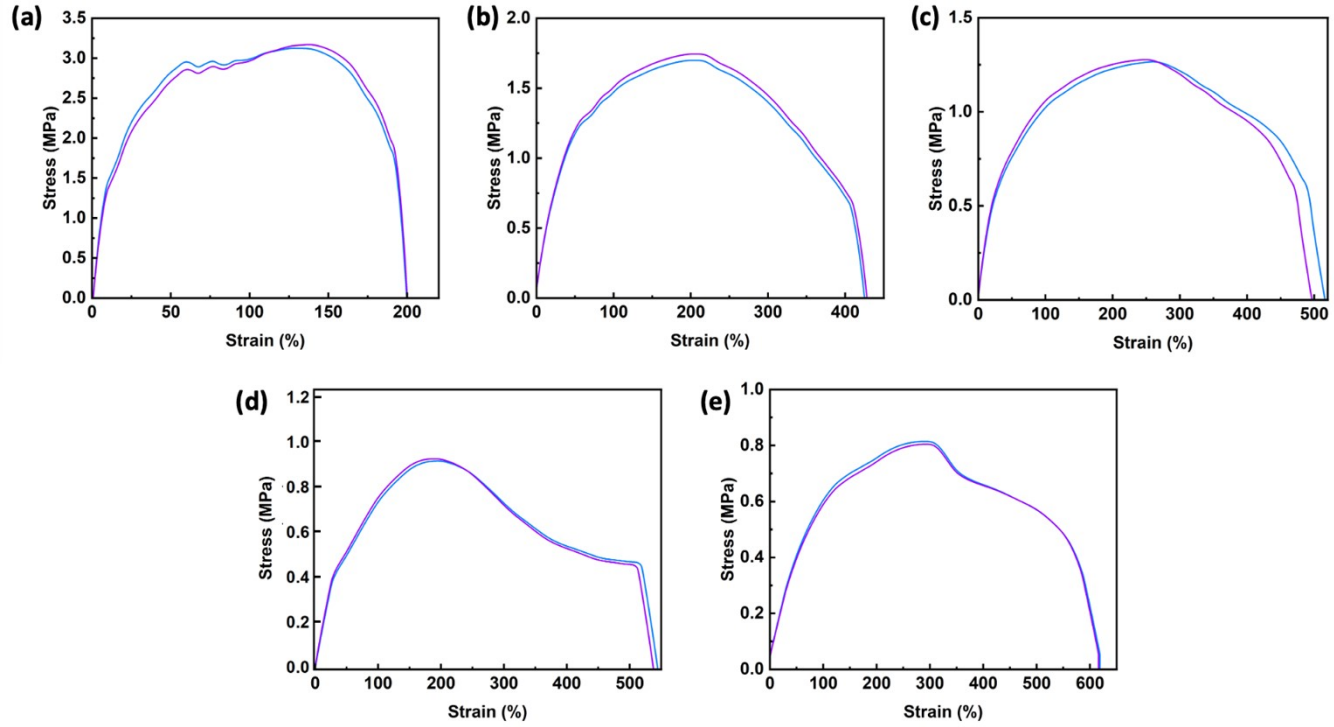

Figure S3. Tensile stress-strain curve for PEDOT:PSS/PU-based films: (a) PEDOT:PSS/PU-13, (b) PEDOT:PSS/PU-15, (c) PEDOT:PSS/PU-18, (d) PEDOT:PSS/PU-15/Gly-2.4, and (e) PEDOT:PSS/PU-18/Gly-2.2. Two measurements for each sample are shown.

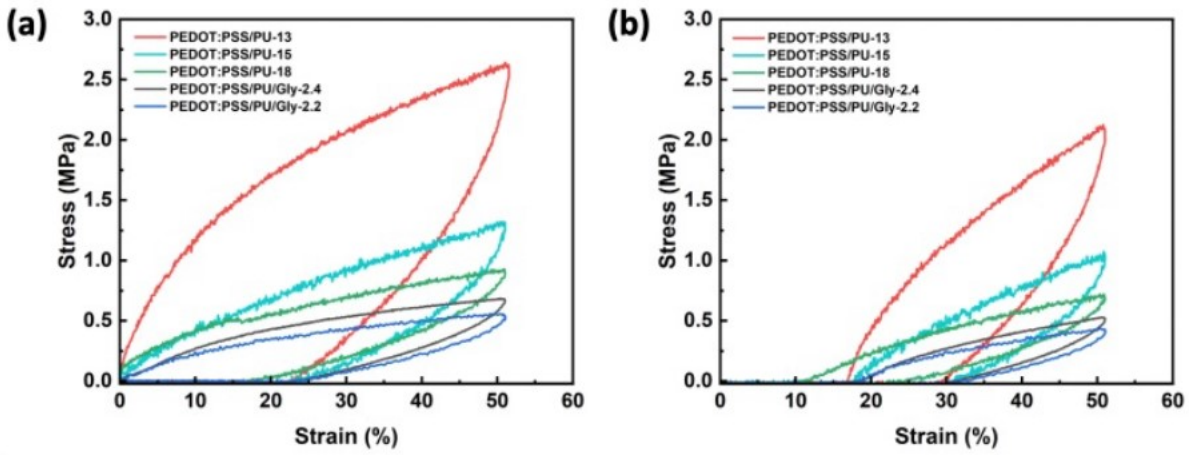

Figure S4. Tensile loading–unloading curves of PEDOT:PSS/PU-based films recorded during (a) the 1st cycle and (b) the 500th cycle over a strain range of 0–50%.

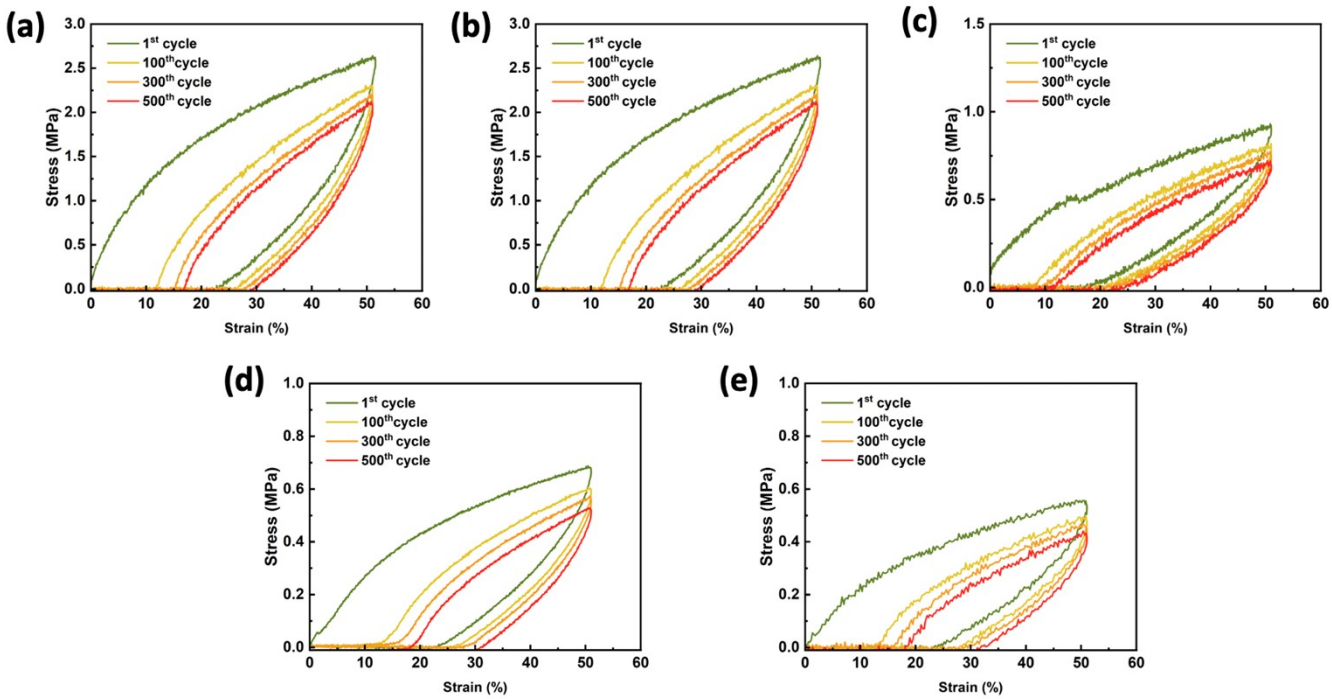

Figure S5. Tensile loading–unloading curves of (a) PEDOT:PSS/PU-13, (b) PEDOT:PSS/PU-15, (c) PEDOT:PSS/PU-18, (d) PEDOT:PSS/PU-15/Gly-2.4, and (e) PEDOT:PSS/PU-18/Gly-2.2 films recorded during the 1st, 100th, 300th, and 500th tensile cycles over a strain range of 0–50%.

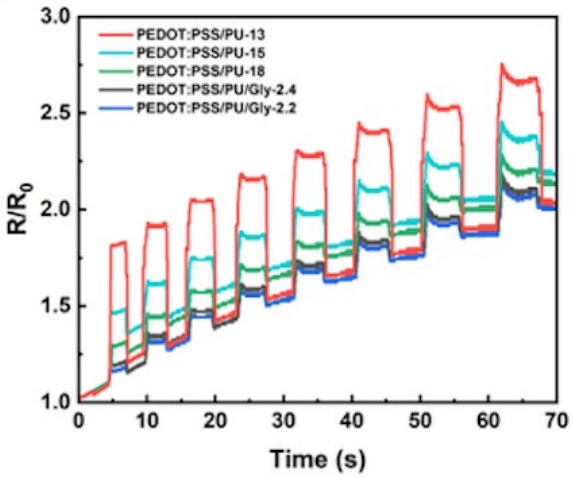

Figure S6. Normalized resistance change (R/R_o) measured under a constant 0.2 V bias as a function of tensile strain, incrementally increased from 50% to 400% in 50% steps at a stretching rate of 10 mm min^{-1}.

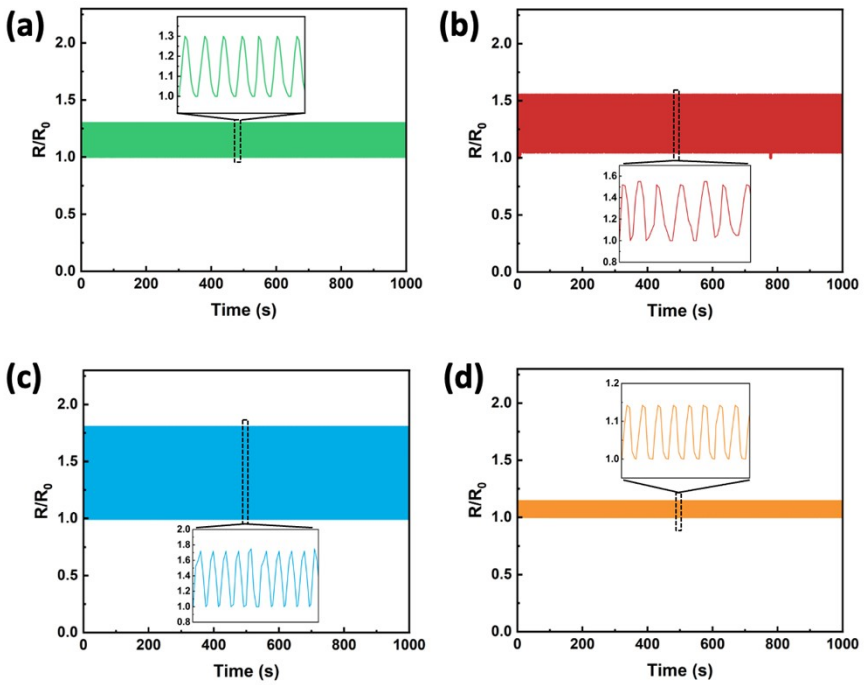

Figure S7. Normalized resistance change (R/R_o) as a function of time during 500 cyclic tensile strain cycles (0–50%) for (a) PEDOT:PSS/PU-13, (b) PEDOT:PSS/PU-15, (c) PEDOT:PSS/PU-18, and (d) PEDOT:PSS/PU/Gly-2.4 films. The insets show a magnified view of cycles 500–530, highlighting resistance fluctuations during cyclic deformation.

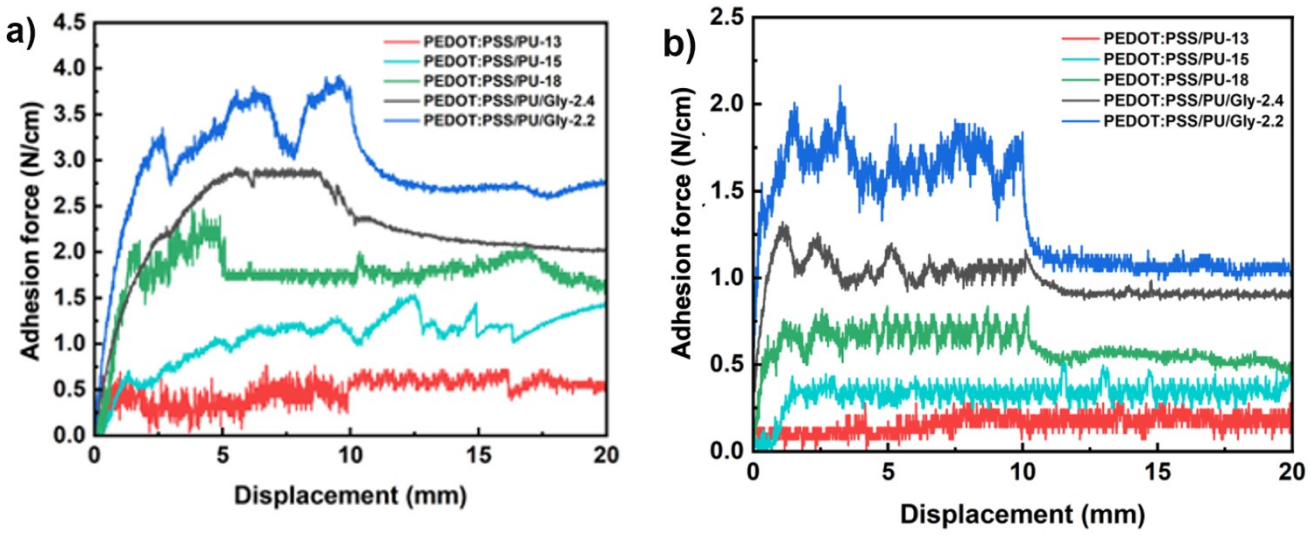

Figure S8. Adhesion strength of PEDOT:PSS/PU-based films measured on film-to-film self-adhesion interfaces (a) and glass substrates (b).

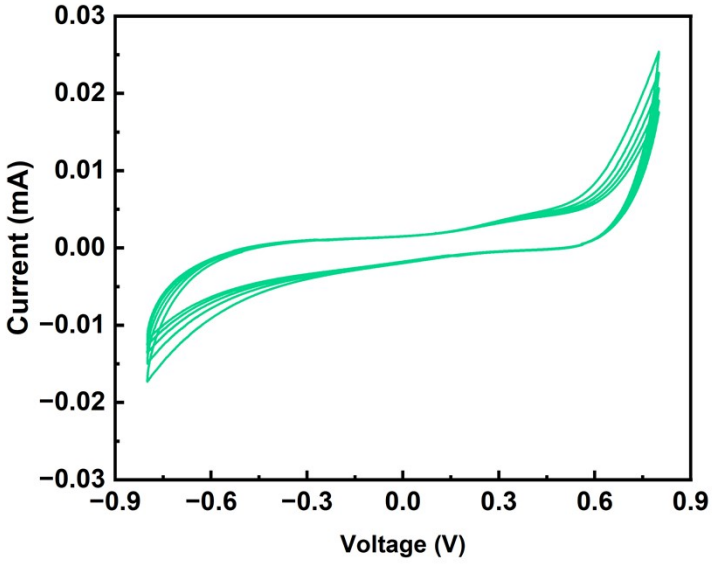

Figure S9. Cyclic voltammetry (CV) curves of PEDOT:PSS/PU-18-Gly2.2 measured at a scan rate of 10mV/s.

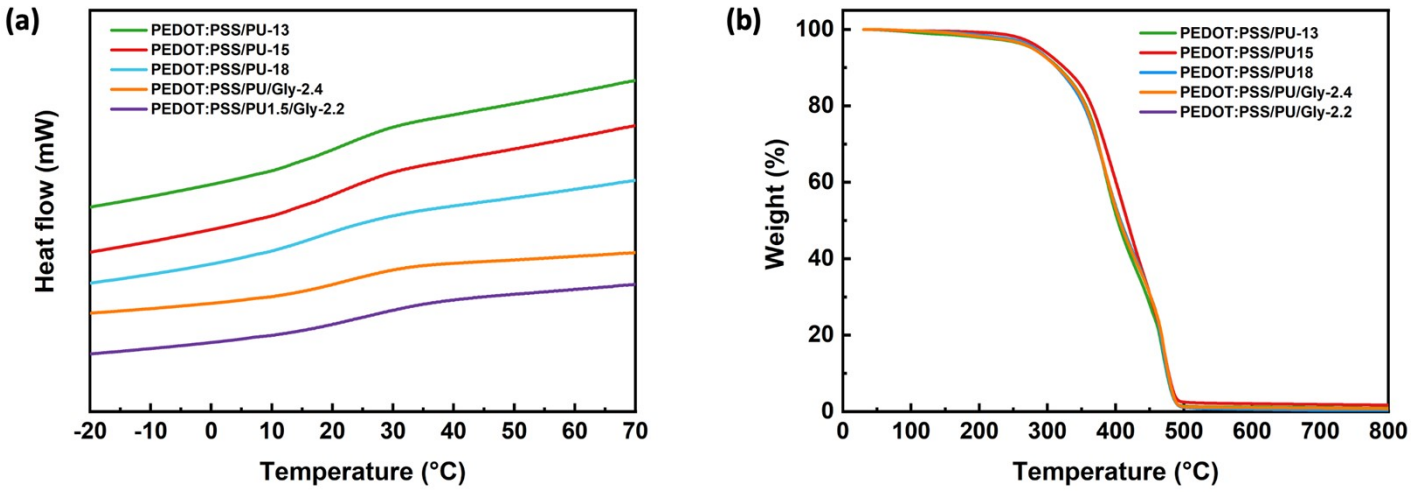

Figure S10. (a) DSC and (b) TGA thermograms of PEDOT:PSS/PU-based films.

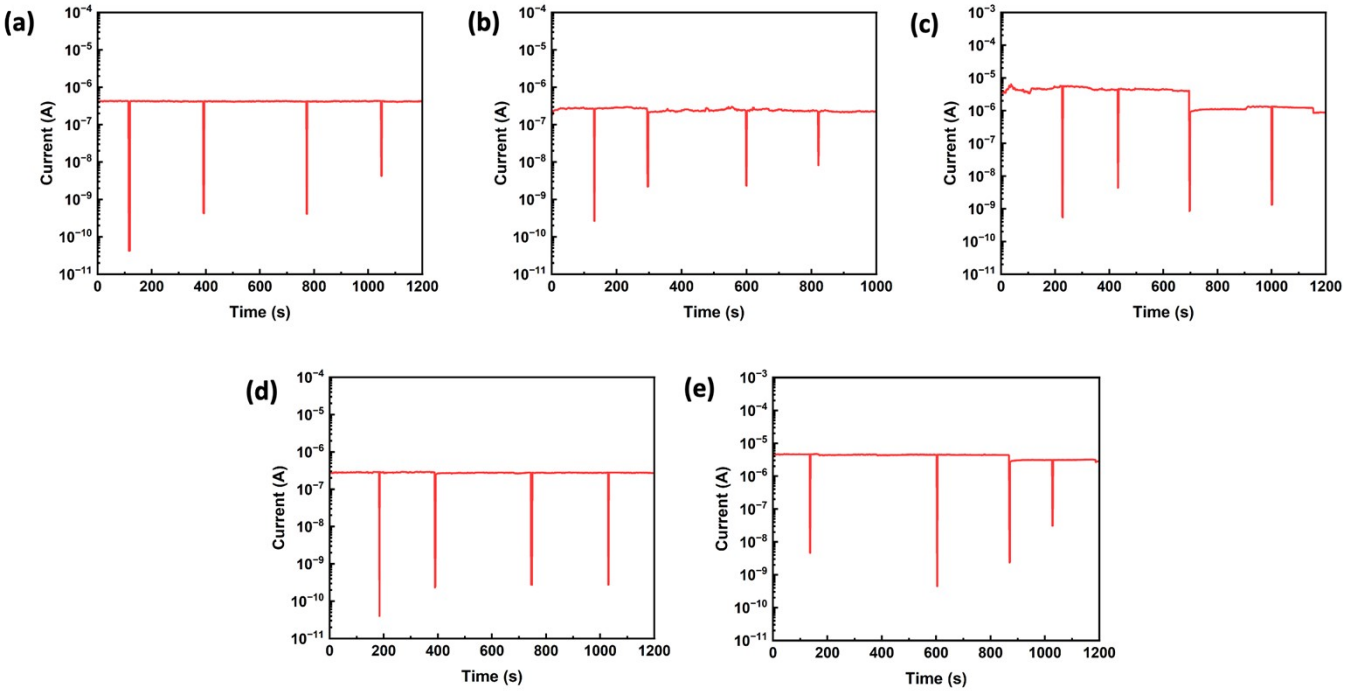

Figure S11. Current–time responses of drop-cast (a) PEDOT:PSS/PU-13, (b) PEDOT:PSS/PU-15, (c) PEDOT:PSS/PU-18, (d) PEDOT:PSS/PU-15/Gly-2.4, and (e) PEDOT:PSS/PU-18/Gly-2.2 films recorded during repeated cut–and–heal cycles under a constant 0.2 V bias.

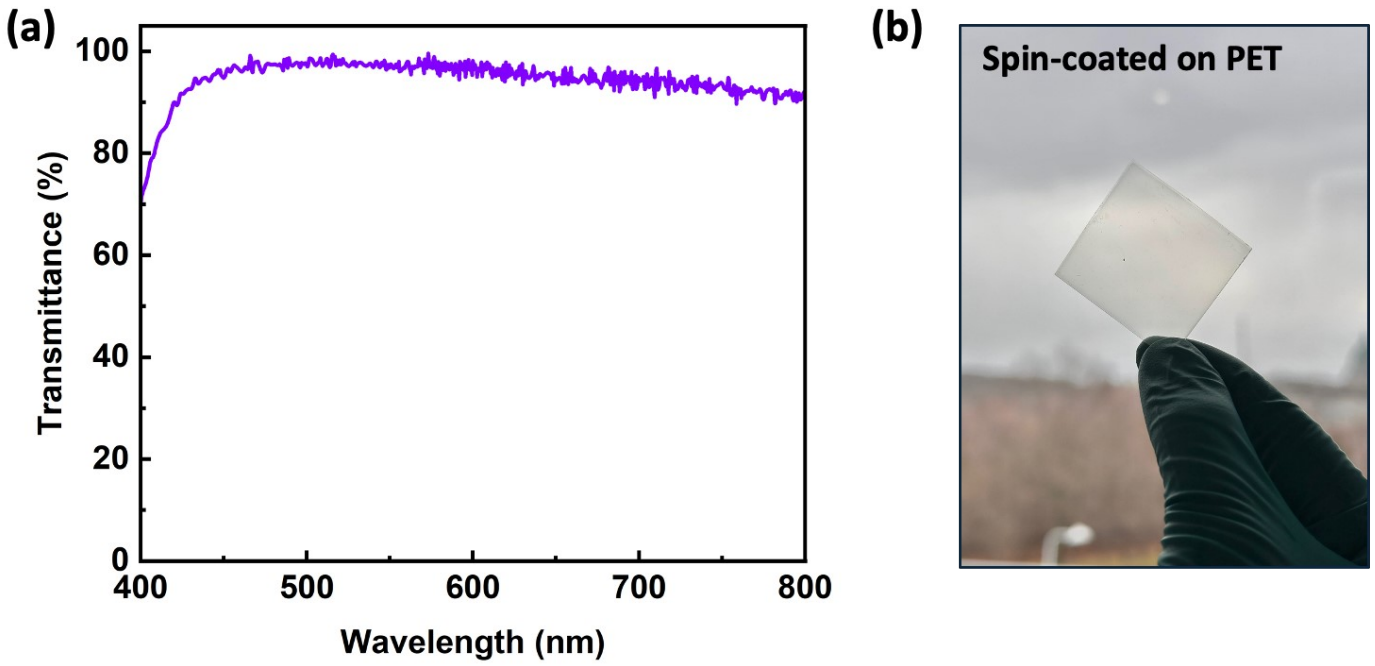

Figure S12. (a) UV-Vis transmittance spectrum of a spin-coated PEDOT:PSS/PU-18/Gly-2.2 film on glass in the wavelength range 400-900 nm, with the corresponding photograph. (b) Photograph of a spin-coated PEDOT:PSS/PU-18/Gly-2.2 film on a PET substrate.

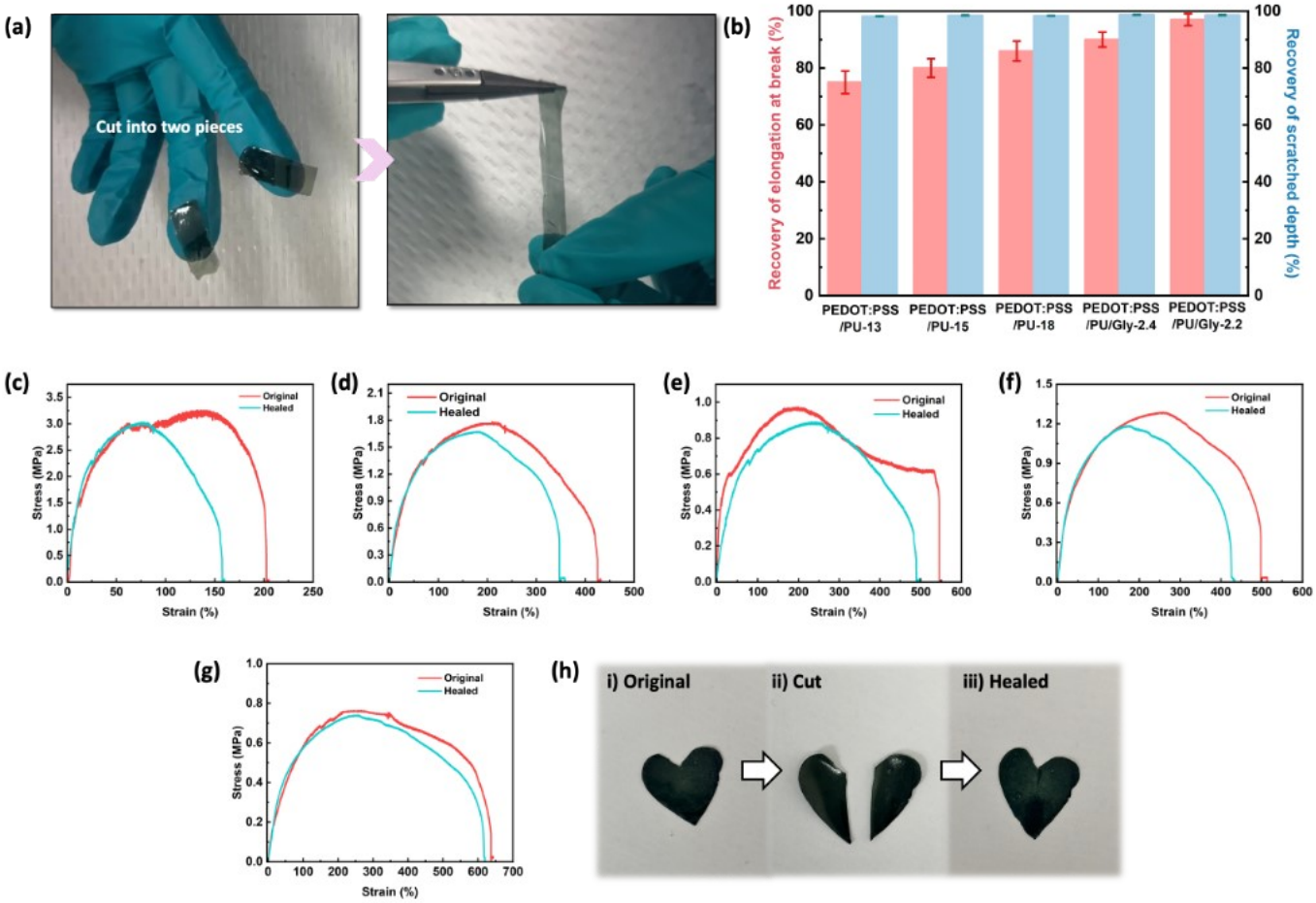

Figure S13. (a) Photographs illustrating the cut–stick self-healing test procedure. (b) Average healing efficiencies calculated from recovery of elongation at break and scratch depth for PEDOT:PSS/PU-based films. Stress–strain curves of (c) PEDOT:PSS/PU-13, (d) PEDOT:PSS/PU-15, (e) PEDOT:PSS/PU-18, (f) PEDOT:PSS/PU-15/Gly-2.4, and (g) PEDOT:PSS/PU-18/Gly-2.2 films in their original (red) and healed (blue) states following cut–stick self-healing at room temperature. (h) Representative images of PEDOT:PSS/PU-18/Gly-2.2 films showing the original state, the cut state, and the healed state.

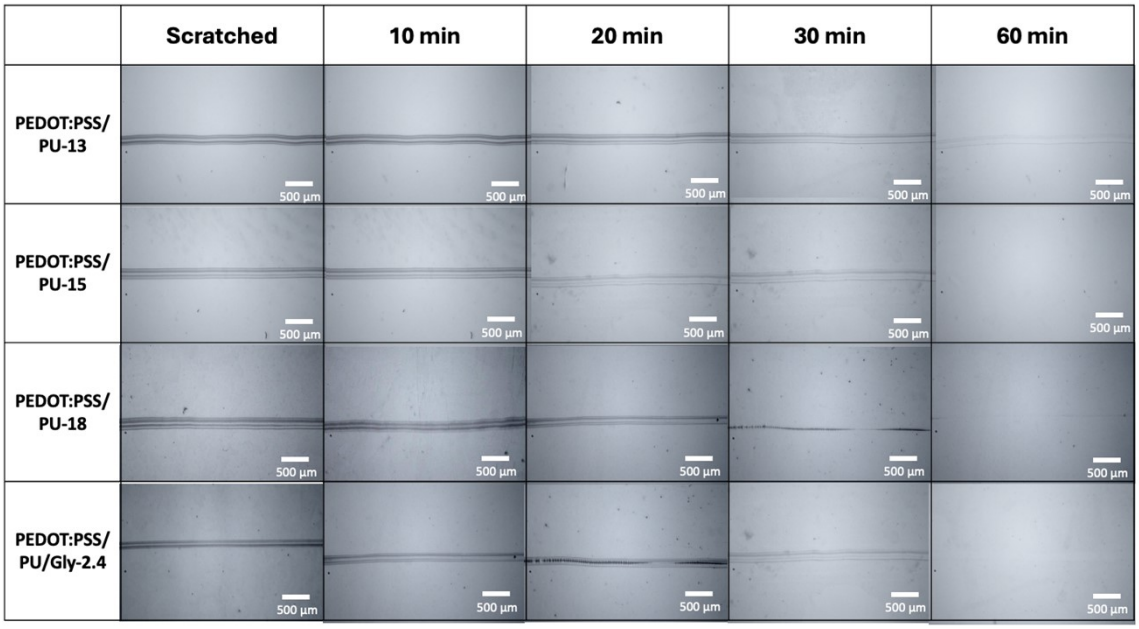

Figure S14. Optical microscope images showing induced damage and subsequent healing of PEDOT:PSS/PU composite films.

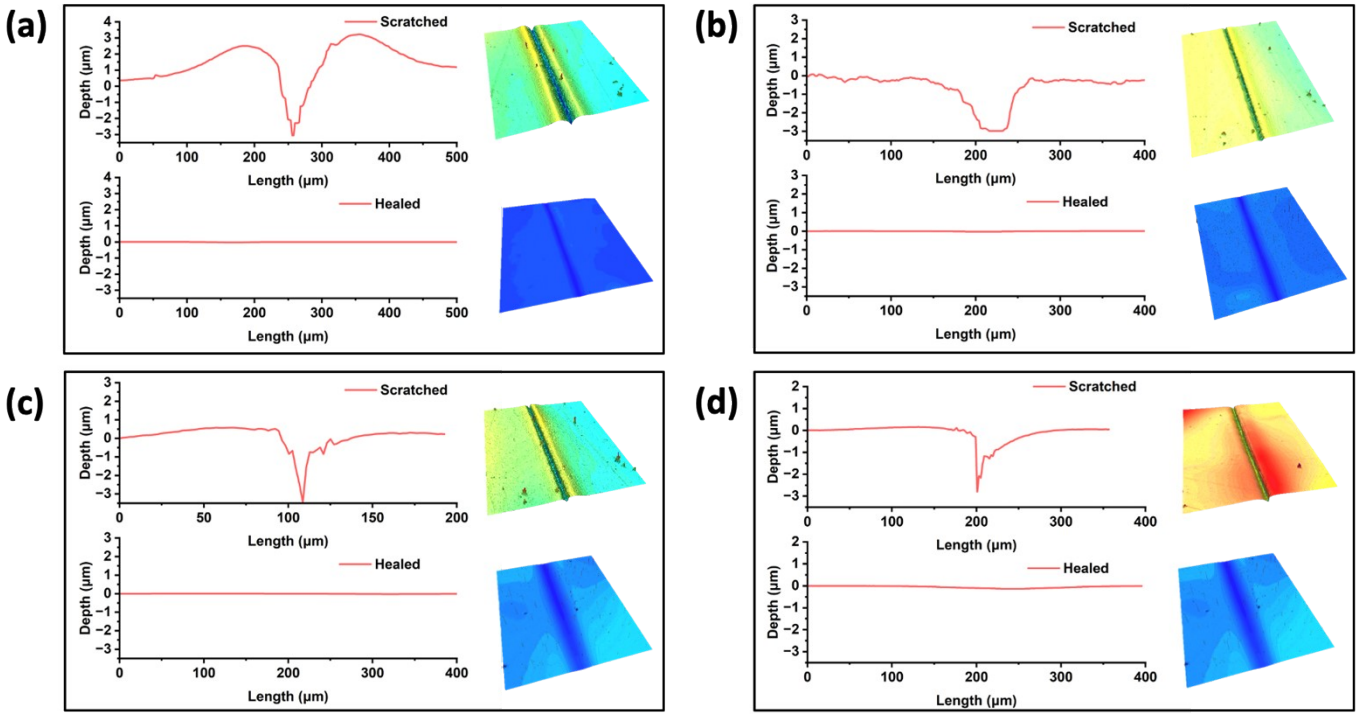

Figure S15. Surface depth profiles and 3D optical profilometry images of (a) PEDOT:PSS/PU-13, (b) PEDOT:PSS/PU-15, (c) PEDOT:PSS/PU-18, and (d) PEDOT:PSS/PU-15/Gly-2.4 films after pencil-induced surface scratching with pencil and subsequent healing at room temperature.

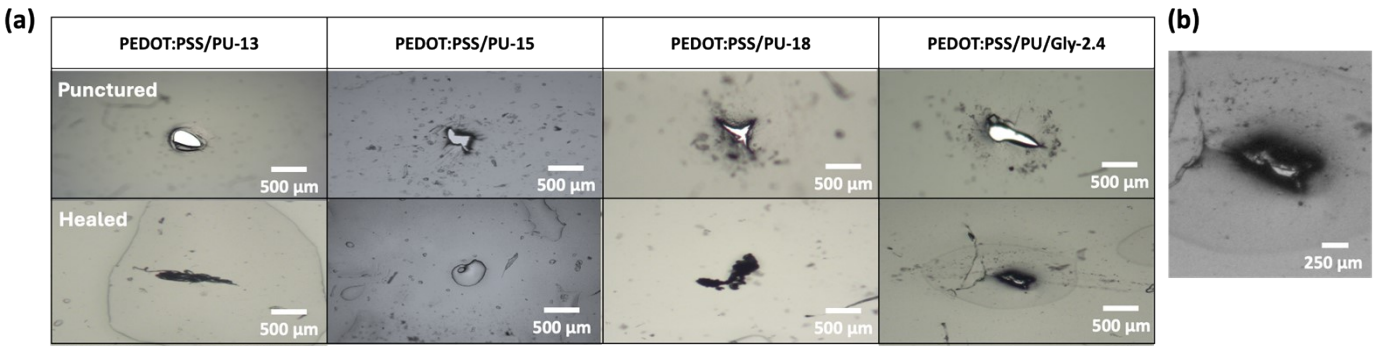

Figure S16. Optical microscope images of (a) PEDOT:PSS/PU-based membranes after puncture and subsequent healing at room temperature and (b) magnified view of the healed region in a PEDOT:PSS/PU/Gly-2.2 film.

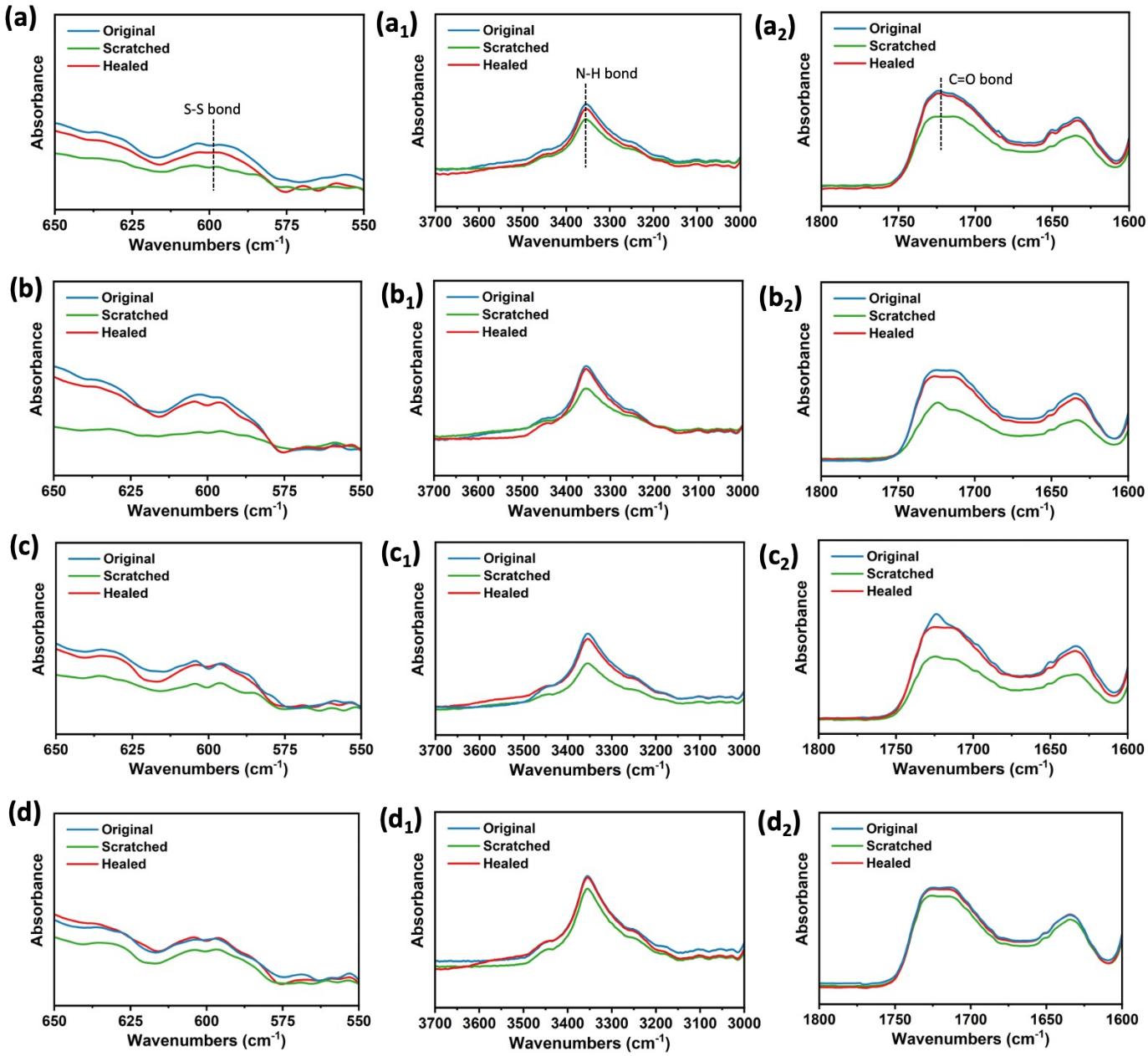

Figure S17. Solid-state FTIR spectra of (a_1-a_3) PEDOT:PSS/PU-13, (b_1-b_3) PEDOT:PSS/PU-15, (c_1-c_3) PEDOT:PSS/PU-18, and (d_1-d_3) PEDOT:PSS/PU-15/Gly-2.4 films recorded in their original, scratched, and healed states. The spectral regions highlight the characteristic vibrational bands corresponding to S-S stretching (a-e), C=O stretching (a_1-e_1), and N-H stretching (a_2-e_2).

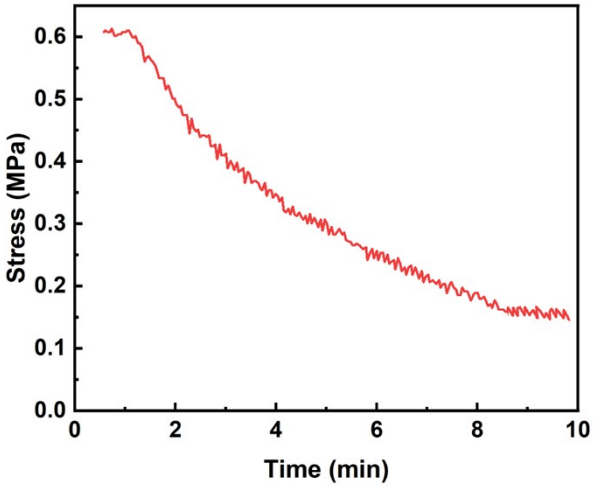

Figure S18. Stress relaxation behavior of PEDOT:PSS/PU-18/Gly-2.2 under constant strain (50%) at room temperature (25 °C).

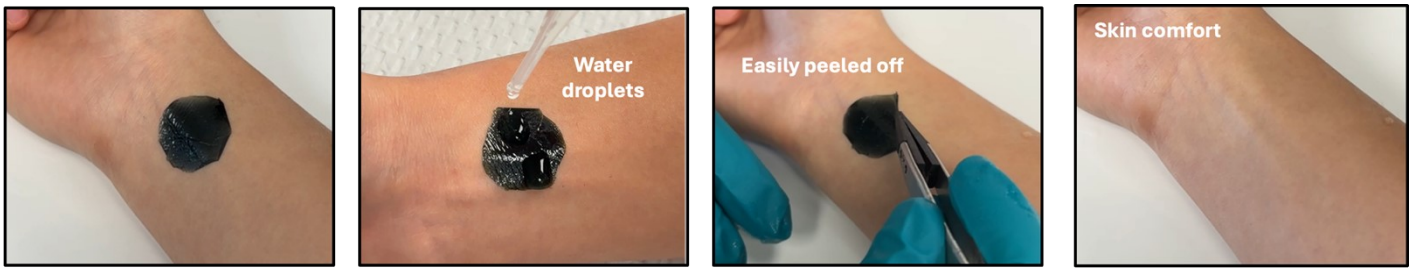

Figure S19. Images showing direct transfer of the freestanding electrode onto skin and its gentle removal using water, without causing skin damage and electrode damage.

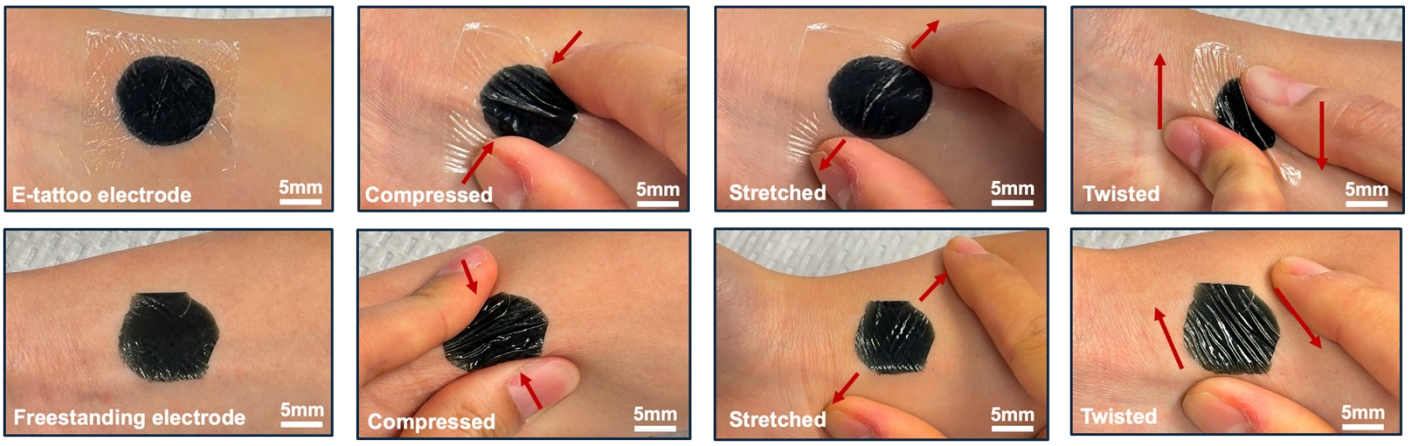

Figure S20. Demonstration of the conformability of e-tattoo and freestanding electrodes on human skin under various mechanical deformations, including compression, stretching, and twisting.

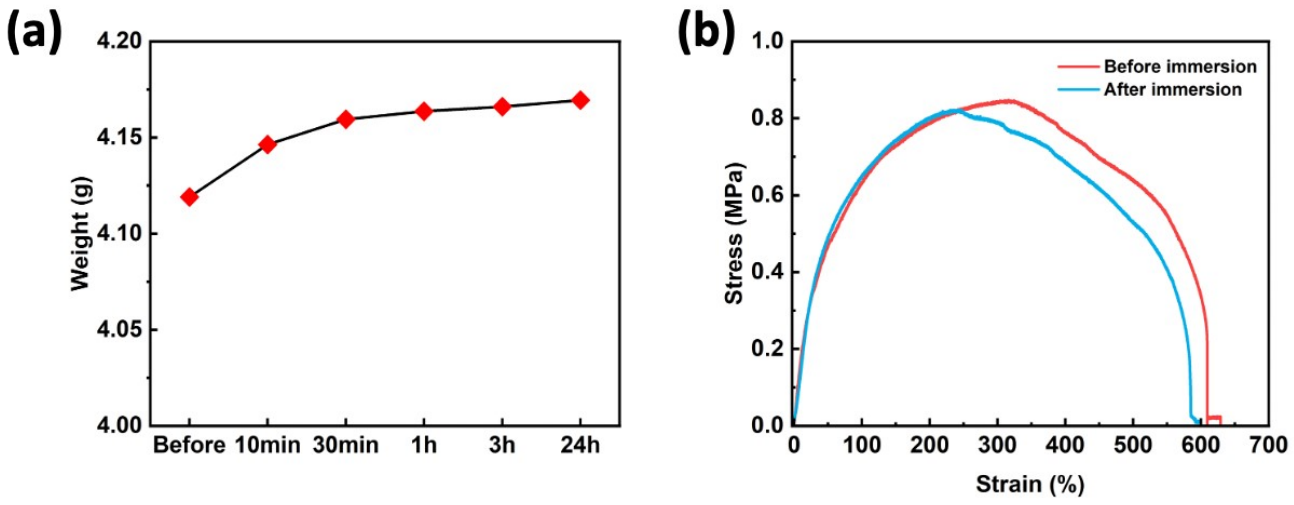

Figure S21. (a) Relative Weight increase of PEDOT:PSS/PU-15/Gly-2.2 films after immersion in water for 24 h, and (b) tensile stress–strain curves of the film measured before and after water soaking.

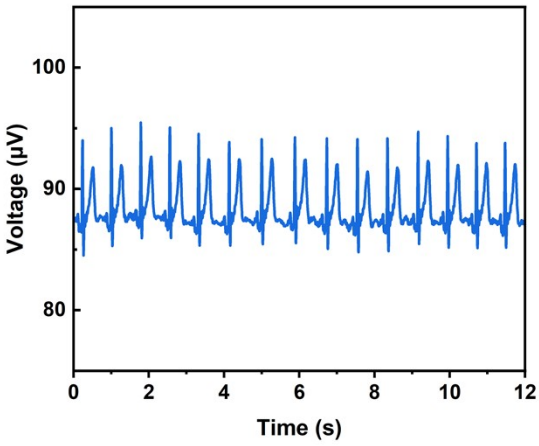

Figure S22. Representative ECG signal recorded using freestanding PEDOT:PSS/PU-18/Gly-2.2 electrodes after reuse.

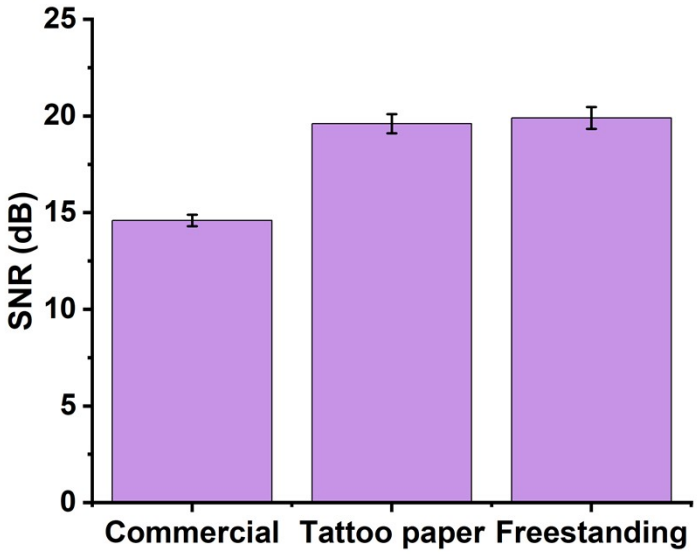

Figure S23. Signal-to-noise ratio (SNR) of ECG signals recorded using commercial, tattoo, and freestanding electrodes. Error bars represent standard deviation (n = 4).

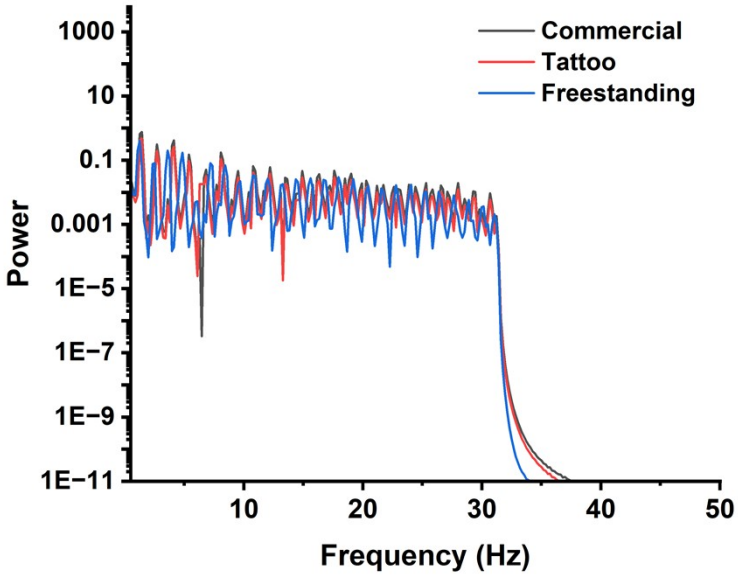

Figure S24. Power spectra of ECG signals recorded using commercial, tattoo, and freestanding electrodes. Data (n = 4) show comparable spectral distributions across the ECG-relevant frequency range.

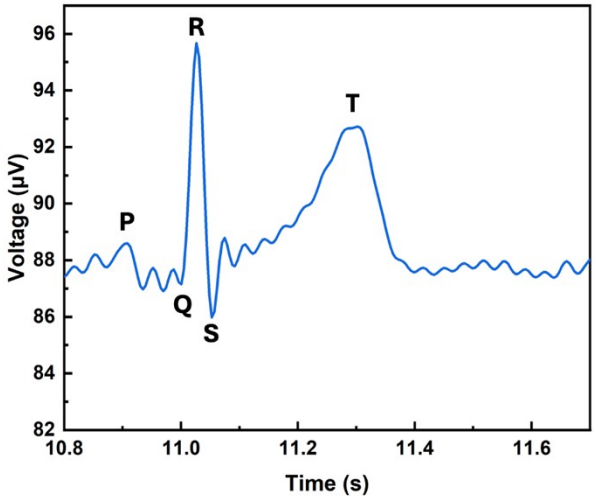

Figure S25. Representative ECG signals recorded using a freestanding PEDOT:PSS/PU-18/Gly-2.2 electrode. Well-defined P, Q, R, S, and T waves are clearly resolved in both cases, confirming stable and high-quality biosignal acquisition.

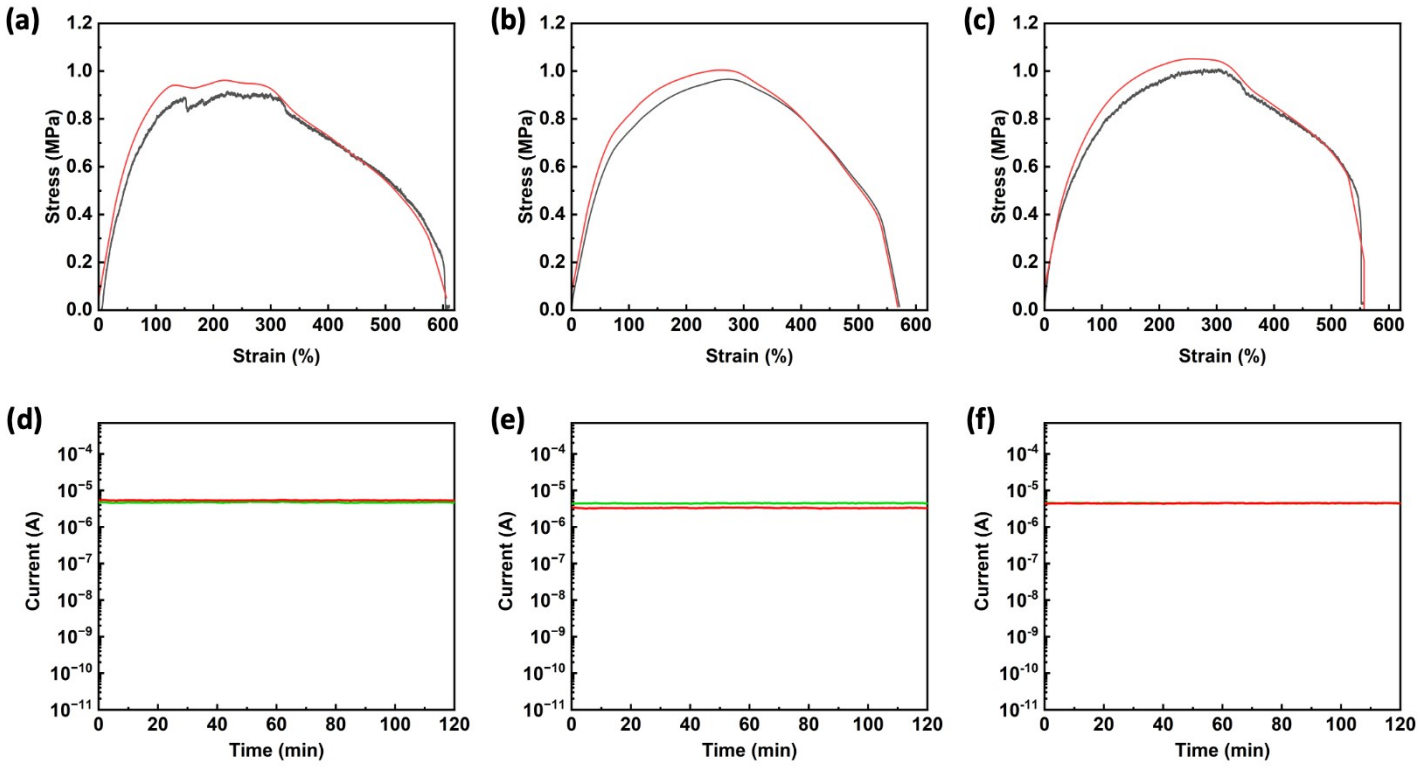

Figure S26. Tensile stress–strain curves and current–time responses of the original and recycled films, demonstrating recovery of mechanical and electrical performance after multiple recycling cycles used for Figure 6. All electrical and mechanical data were collected over 15 recycling cycles, with prepared samples measured in each cycle to confirm reproducibility: (a, d) original, (b, e) after chemical recycling, and (c, f) after mechanical recycling.

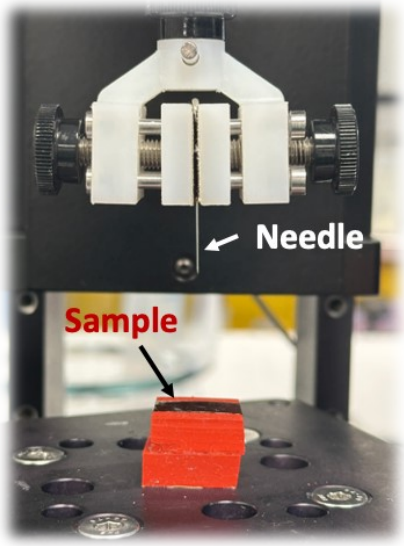

Figure S27. Setup for the puncture healing experiment.

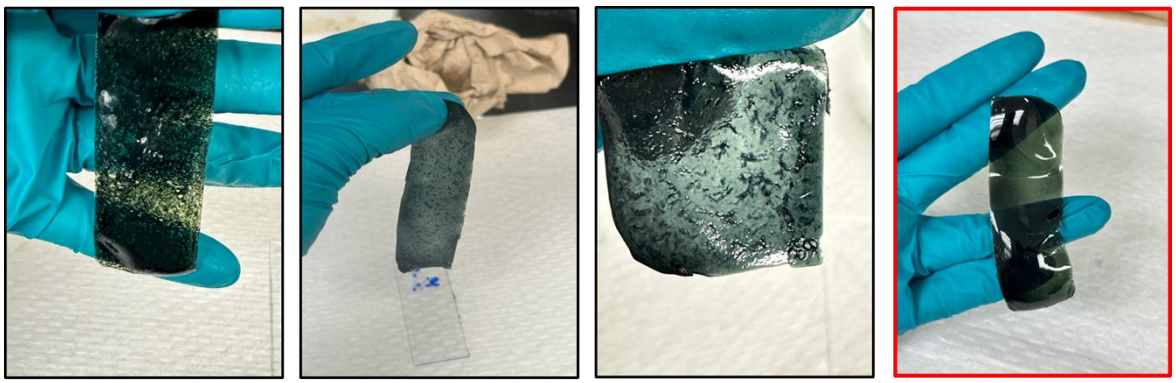

Figure S28. Image of PEDOT:PSS/PU-18/Gly-2.2 drop cast films prepared using different solvents.

Solvents	Solubility of PU	Solubility of PEDOT:PSS (SV3)
Acetonitrile	**O**	**△**
IPA	**O**	**△**
EtOH	**O**	**O**
Anisole	**O**	**X**

Table S1. Solubility test of PU and PEDOT:PSS (SV3) in different solvents. Symbols denote the dissolution response of the samples: O = complete dissolution, △ = partial dissolution, and X = no dissolution.

Samples	Ultimate tensile strength (MPa)	Elongation at break (%)	Young's modulus (MPa)
Original	0.76±0.12	630±19	0.02±0.002
After chemical recycling	0.77±0.21	520±8	0.02±0.001
After mechanical recycling	0.82±0.21	512±5	0.02±0.002

Table S2. elongation at break and Young's modulus (measured in the 0–10% strain range) of PEDOT:PSS/PU-18/Gly-2.2 films after recycling. Data are reported as the mean ± standard deviation, with each sample measured three times (n = 3).

Category	This work	Ref 1 (Graphene/ CNF)	Ref 2 (PEDOT:PAAM PSA:PA)	Ref 3 (CB/CNT/PU)	Ref 4 (PAA/Al/PQ hydrogel)	Ref 5 (Boroxine/ PU)	Ref 6 (WPU/ PPy)	Ref 7 (PEDOT:PS S/PU/PEG)
Elongation at break	630%	1000%	1050%	245%	1400%	500%	597%	350%
Mechanical Healing efficiency	98%	-	92%	87%	50%	94%	83%	90%
Healing time	1 h	24 h	2 h	7 min	24 h	1 h	1 h	10 min
Type of healed damage	Cut, Scratch, Puncture	Cut, Scratch	Cut	Cut	Cut	Cut, Scratch	Cut	Cut, Scratch
Healing Temp.	r.t	r.t	r.t	70 °C	r.t	r.t	60 °C	50 °C
Recyclability	Yes (Chemical & Mechanical)	Yes (Mechanical)	No	Yes (Chemical)	Yes (Mechanical)	Yes (Mechanical)	Yes (Mechanical)	Yes (Mechanical)
Processing	Drop-cast Spin-coating Printing	Spin-coating	Drop-cast Spin-coating	Hot pressing	Drop-cast	Drop-cast	Drop-cast	Drop-cast
Conductivity	14 S/cm	0.309 S/cm	0.309 S/cm	8.20 S/cm	0.006 S/cm	-	-	10 S/cm

Table S3. Comparison of key electromechanical, self-healing, and recyclability properties of the PEDOT:PSS/PU composite developed in this work with recently reported self-healing conductive materials.

References

1. C. Zheng, Y. Yue, L. Gan, C. Mei and J. Han, Highly Stretchable and Self-Healing Strain Sensors Based on Nanocellulose-Supported Graphene Dispersed in Electro-Conductive Hydrogels Nanomaterials, 2019, 9(7), 937. http://doi.org/10.3390/nano9070937.
2. D. Kim, Z. A. Akbar, Y. T. Malik, J. Jeon and S. Jang, Self-healable polymer complex with a giant ionic thermoelectric effect, Nature Communications, 2023, 14, 3246. https://doi.org/10.1038/s41467-023-38830-w
3. Y. Wang, B. Park, V. Vu, and S. Lee, Polymer Engineering & Science, 2025, 65(4), 1854-1867. Self-healing conducting composite electrodes derived from chemical recycling of PET plastic wastes for flexible supercapacitors. https://doi.org/10.1002/pen.27117
4. J. Zou, Z. Yang, J. Liang, Y. XIe, M. Fan and X. Zhang, Polymer, 2024, 315, 127826. Key Mechanisms Mechanically Improve Polyacrylamide-Based Hydrogels. https://doi.org/10.1002/pol.20250252
5. H. Mao, Y. Zhang, L. Zhao, H. Li, H. Wu and L. Lin, ACS Applied Polymer Materials, 2024, 7(1), 164-174. Dynamic bond-enhanced, recyclable polyurethane elastomer with high strength and self-healing properties for advanced 3D printing. https://doi.org/10.1016/j.compositesb.2025.112500
6. K. Zhu, L. Yang, X. Zhou, X. Zhang, Y. Hao, F. Li, W. Lei, Q. Wang and G. Wang, Chemical Engineering Journal, 2025, 510, 161515. Self-healing watervorne polyurethane originated from waste PET and their composites with polypyrrole for stretchable strain sensor. https://doi.org/10.1016/j.cej.2025.161515
7. J. Kim, J. X. Fan, G. Petrossian, X. Zhou, P. Kateb, N. Gagnon-Lafrenais and F. Cicoira, Mater Horiz, 2024, 11. https://doi.org/10.1039/D4MH00203B